A new two-scale model describing drying dynamics and coupled heat and mass transfer in a porous medium: application to the combined vacuum drying and radiative heating of wood

Ian Turner, Patrick Perré

Drying 2004 – Proceedings of the 14th International Drying Symposium (IDS 2004)
São Paulo, Brazil, 22-25 August 2004, vol. A, pp. 436-443

A NEW TWO-SCALE MODEL DESCRIBING DRYING KILN DYNAMICS AND COUPLED HEAT AND MASS TRANSFER IN A POROUS MEDIUM: APPLICATION TO THE COMBINED VACUUM DRYING AND RADIATIVE HEATING OF WOOD

Ian Turner[1] and Patrick Perré[2]

1. School of Mathematical Sciences, Queensland University of Technology, GPO Box 2434, Brisbane, Q4001, Australia
2. LERMAB (laboratory of Wood Science), UMR 1093 INRA/ENGREF/ Université Henry Poincaré, ENGREF – 14 rue Girardet, F-54042 Nancy Cedex – France, Email: perre@engref.fr

Keywords: Two-dimensional heat and mass transfer, vacuum chamber model, experimental data, kiln-load coupling

ABSTRACT

In this work a two-scale modelling approach is used to investigate the vacuum drying of a board placed in an experimental vacuum chamber, whereby two infrared emitters with reflectors are used to supply heat to the product. The kiln (large) scale model allows the evolution of the masses of vapour, air and water in the chamber, together with the temperatures of the vacuum chamber and the IR emitters to be monitored throughout the drying process. Such a model enables condensation on the kiln walls to be accounted for in the evolution of the relative humidity within the chamber. The comprehensive two-dimensional drying model, known as *Transpore*, is used to determine the heat and mass transfer at the (macro) scale of the board. The knowledge of the vacuum chamber vapour pressure at any given instant using the large-scale model enables the intricate coupling that exists between the wood and the chamber to be realised throughout the simulation. This innovative modelling approach provides a precise description of the experimental configuration for which the model can be verified. Finally, two case studies are presented to elucidate the coupling that exists between the technical specifications of the chamber and the drying mechanisms in the porous medium.

INTRODUCTION

A primary attraction of vacuum drying is the reduced drying times and higher end product quality that it offers in comparison with conventional drying operations (Ressel 1994). In fact, operating at low pressures provides a reduction in the boiling point of water, which in turn enables an important overpressure that drives moisture efficiently from the board to be generated and maintained within the product throughout drying. For some wood species that can not withstand high temperature conditions,

vacuum drying offers the perfect mechanism to avoid collapse and discoloration. As a consequence of these benefits, research in this field is currently receiving significant worldwide attention, especially for high quality hardwoods that are difficult to dry conventionally such as Oak (Joyet and Meunier, 1996, Resch and Gaustch, 2001) and Australian Eucalyptus (Rozsa and Avramindis, 1996).

The effect of reducing the external pressure during drying on the transfer phenomena evolving within wood is quite complex (Bird *et al.* 1960, Masson and Malinauskas 1983, Froment and Bischoff 1990, Perré et *al.* 1995). In particular, one notes the increase of internal transfers due to the increased total gaseous pressure gradients within the board, and the lowering of external exchanges, especially for the heat supplied to the material by the convective flow. It is the lowering of the external energy transfer that still remains the problem to be solved. To overcome this problem, conventional vacuum dryers either use a discontinuous process of alternating phases of vacuum drying with phases of convective heating under atmospheric pressure, or dry under vacuum with heated plates positioned between boards (Joly and More Chevalier, 1980). More recently, other strategies have been devised for supplying energy to the product, for example, high vacuum drying (Joyet and Meunier, 1996), or radio frequency heating, which is optimal in terms of process control, delivers the pressure level and the heat supplied to the load independently (Avramidis, 1999). The work proposed here concerns vacuum drying with radiative heating. This particular strategy for supplying energy to the product is very commonly used in the paper industry, but seldom used for wood drying. This fact is due to the geometry of the stacks, which are not readily adapted to this type of heating. However, radiative devices arranged between layers of boards could offer better performances when compared with heated plates. In particular, contrary to heated plates, it would be possible to design the radiative devices in such a way that the path for the moisture remains free at the surface of the boards.

This work sees the development of a coupled two-scale computational model that can be used to predict the vacuum drying of wood placed in a small prototype industrial dryer. The kiln scale model allows the evolution of the masses of vapour, air and water in the chamber, together with the temperatures of the vacuum chamber and the IR emitters to be monitored throughout the drying process. Such a model enables condensation on the kiln walls to be accounted for in the evolution of the relative humidity within the chamber. The inclusion of this phenomenon within the kiln scale model opens the door for it to be used across a wide range of drying processes and most importantly, allows the notion of online kiln control to become a reality. The knowledge of the vacuum chamber vapour pressure at any given instant throughout the simulation enables the intricate coupling that exists between the wood and the chamber to be realised throughout drying. Finally, the link between the two scales is achieved via the boundary conditions that are imposed at the surface of the porous medium

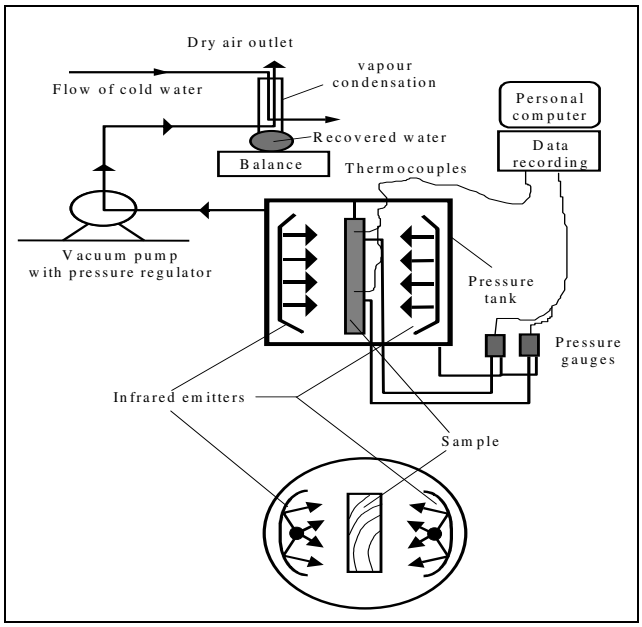

Figure 1 – Vacuum drying configuration.

EXPERIMENTAL CONFIGURATION

Vacuum drying experiments were carried out in the Laboratory of Forest Sciences, ENGREF in France (see Perré, Turner and Mosnier, 2004 for full details). A board was placed into a pressure tank between two IR emitters with reflectors as shown in Figure 1. Far IR radiation (temperature close to 600 K) was obtained by supplying

classical quartz tubes with low voltage. A membrane vacuum pump, with moving parts made from Teflon, able to pump full water vapour from the chamber was used for the experiment. This type of pump allows for the condensation of water at the outlet of the pump, which can subsequently be collected and weighed to determine the moisture removed from the board during drying. By taking some precautions, such as heating the tank walls to avoid condensation, it was possible to recover on the balance up to 95% of the weight loss of the board. Note that the whole condenser is put on the balance so that water can be detected at the instance the vapour appears without the need to wait for the liquid to flow into the receptacle

MATHEMATICAL FORMULATION

Vacuum Chamber Model

Assuming that the pressure and temperature fields within the chamber are homogeneous and taking a control volume that includes the surfaces of the wood sample, together with the walls of the vacuum chamber and the IR emitters, it is possible to derive the following balance equations for the vacuum chamber:

Air Mass Balance

$$\frac{dm_a}{dt} = -\rho_a^{(ch)} Q_{pump} + F_a^{(wood)} A^{(ws)} \tag{1}$$

Vapour Mass Balance

$$\frac{dm_v}{dt} = -\rho_v^{(ch)} Q_{pump} + F_v^{(wood)} A^{(ws)} + F_w^{(ch)} A^{(ev)} \tag{2}$$

Water Mass Balance

$$\frac{dm_w}{dt} = F_w^{(wood)} A^{(ws)} + \begin{cases} F_w^{(ch)} A^{(ch)}, & if\ \ condensation\ \ state \\ -F_w^{(ch)} A^{(ev)}, & if\ \ \ evaporation\ \ state \end{cases} \tag{3}$$

In the mass balance equations (1)-(3), the variables m_a, m_v and m_w represent respectively the masses of air, vapour and water in the chamber and $\rho_a^{(ch)}$ and $\rho_v^{(ch)}$ represent the densities of air and vapour in the chamber. Q_{pump} is the flow rate of the pump, $F_a^{(wood)}$, $F_v^{(wood)}$ and $F_w^{(wood)}$ are the total fluxes of air, vapour and liquid leaving the board and $A^{(ws)}$ is the total surface area of the board. $F_w^{(ch)}$, $A^{(ch)}$ and $A^{(ev)}$ are respectively the fluxes of water in the chamber generated due to condensation or evaporation, the surface area of the vacuum chamber and the total surface area within the chamber open for evaporation, which in this case is the circular bottom of the vacuum chamber.

Chamber Energy Balance

$$\begin{aligned} \frac{d}{dt}\left(m_a e_a + m_v e_v + m_w e_w + m_{ch} e_{ch}\right) = &-\left(\rho_a^{(ch)} h_a + \rho_v^{(ch)} h_v\right) Q_{pump} + F_H A^{(ws)} + \\ &\left(F_{ch\to IR}\sigma\left(T_{IR}^4 - T_{ch}^4\right) + F_{ch\to w}\sigma\left(T_{w_{eq}}^4 - T_{ch}^4\right) + h\left(T_{ext} - T_{ch}\right)\right) A^{(ch)} \end{aligned} \tag{4}$$

Emitter Energy Balance

$$\frac{d}{dt}\left(m_{IR} e_{IR}\right) = \left(F_{IR\to ch}\sigma\left(T_{ch}^4 - T_{IR}^4\right) + F_{IR\to w}\sigma\left(T_{w_{eq}}^4 - T_{IR}^4\right)\right) A^{(IR)} + E_{pwr} \tag{5}$$

In the energy balance equations (4) and (5), m_{ch} and m_{IR} represent the masses of the chamber walls and the IR emitters and $A^{(IR)}$ represent the surface area of the IR emitter. T_{ch} and T_{IR} are the temperatures of the chamber and the IR emitters and e_a, e_v, e_w, e_{ch} and e_{IR} are the internal specific energies of the air, vapour, water, chamber and IR emitters. h_a and h_v are the specific enthalpies of the air and vapour in the chamber and F_H is the total convective heat flux from the board to the chamber. E_{pwr} represents the input electrical power of the system, σ the Stefan-Boltzmann constant and h the external convective heat transfer coefficient. The view factors $F_{ch\to IR}, F_{ch\to w}, F_{IR\to ch}, F_{IR\to w}$ have been estimated from Bird *et al*. (1960)

for the case of two parallel metal plates. The internal energies of the air and vapour can be written as $e = h - P\nu$, where ν is the specific volume and P pressure. Such a relation allows compressive heating effects to be accounted for within the conservation law. Note that the internal energies and the enthalpies of all other variables are equal.

Pressure in the chamber is computed according to the Ideal gas law. The enthalpies of each phase are computed by assuming that the gas and liquid phases evolving in the chamber equal the chamber wall temperature. The enthalpy of the chamber walls and the IR emitters are assumed to equal the product of the specific heat of stainless steel and temperature. The flux of water in the chamber is controlled using a set of rules that enables a condensation state $P_v^{(ch)} > P_{vs}^{(ch)}$ or an evaporation state to exist.

Wood Transport Model

The macroscopic conservation equations that govern the heat and mass transfer phenomena that arise in porous media during drying are now well known (Whitaker, 1977). These equations have been extended and numerically solved to enable the drying of softwood to be simulated (Perré and Degiovanni 1990, Turner and Perré, 1996; Perré and Turner, 1996, 1997, 1999a, 1999b). The conservation laws for liquid, energy and air are summarised, together with the gas and liquid phase velocities, as follows:

Liquid
$$\frac{\partial}{\partial t}\left(\varepsilon_w\rho_w + \varepsilon_g\rho_v + \overline{\rho}_b\right) + \nabla\cdot\left(\rho_w\overline{\mathbf{v}}_w + \rho_v\overline{\mathbf{v}}_g + \overline{\rho_b\mathbf{v}_b}\right) = \nabla\cdot\left(\rho_g\overline{\overline{\mathbf{D}}}_{eff}\nabla\omega_v\right) \tag{6}$$

Energy
$$\begin{aligned}\frac{\partial}{\partial t}\left(\varepsilon_w\rho_w h_w + \varepsilon_g(\rho_v h_v + \rho_a h_a) + \overline{\rho}_b\overline{h}_b + \rho_o h_s - \varepsilon_g P_g\right) + \nabla\cdot\left(\rho_w h_w\overline{\mathbf{v}}_w + (\rho_v h_v + \rho_a h_a)\overline{\mathbf{v}}_g + h_b\,\overline{\rho_b\mathbf{v}_b}\right)\\ = \nabla\cdot\left(\rho_g\overline{\overline{\mathbf{D}}}_{eff}(h_v\nabla\omega_v + h_a\nabla\omega_a) + \overline{\overline{\mathbf{K}}}_{eff}\nabla T\right)\end{aligned} \tag{7}$$

Air
$$\frac{\partial}{\partial t}\left(\varepsilon_g\rho_a\right) + \nabla\cdot\left(\rho_a\overline{\mathbf{v}}_g\right) = \nabla\cdot\left(\rho_g\overline{\overline{\mathbf{D}}}_{eff}\nabla\omega_a\right) \tag{8}$$

Generalised Darcy's Law
$$\overline{\mathbf{v}}_\ell = -\frac{\overline{\overline{\mathbf{K}}}_\ell\overline{\mathbf{k}}_\ell}{\mu_\ell}\nabla\varphi_\ell \quad , \quad \nabla\varphi_\ell = \nabla P_\ell - \rho_\ell g\nabla\chi \quad \textit{where} \quad \ell = w, g \tag{9}$$

In equation (9) the quantities φ are known as the phase potentials and χ is the depth scalar. The driving potential for the bound liquid migration is assumed to be proportional to a gradient in bound liquid (Perré *et al.,* 1993):

$$\overline{\rho_b\mathbf{v}_b} = -\rho_o\overline{\overline{\mathbf{D}}}_b\nabla X_b \tag{10}$$

Physical Properties

Most of the key parameters that exist within the macroscopic transport equations (6)-(10) are strongly dependent on the structure of the material. These properties, together with their postulated functional dependencies have been taken directly from the literature (see for example Perré and Turner 1996).

Boundary Conditions

The boundary conditions proposed for the external drying surfaces of the wood sample are assumed to have the following form:

$$\begin{aligned}\mathbf{J}_\mathbf{w}\cdot\hat{\mathbf{n}} &= k_m c M_v \ln\left(\frac{1-x_v^{(ch)}}{1-x_v}\right)\\ \mathbf{J}_\mathbf{e}\cdot\hat{\mathbf{n}} &= F_{w\to ch}\sigma\left(T^4 - T_{ch}^4\right) + F_{w\to IR}\sigma\left(T^4 - T_{IR}^4\right) + h_v k_m c M_v \ln\left(\frac{1-x_v^{(ch)}}{1-x_v}\right)\end{aligned} \tag{11}$$

where $\mathbf{J}_\mathbf{w}$ and $\mathbf{J}_\mathbf{e}$ represent the total liquid and energy fluxes through the boundary surfaces and x_v and T are respectively the molar fraction of the gas vapour and the temperature at the exchange surfaces. The corresponding variables with the subscript (ch) indicate quantities that are characteristic of the vacuum

chamber. Consequently, in equation (11) lies one sense of the coupling, from the chamber to the load. The quantity k_m is an appropriately defined mass transfer coefficient and the view factors $F_{w\to ch}$ and $F_{w\to IR}$ have again been estimated. It should be noted that in the case of pure vapour within the chamber, the boundary condition (11) imposes an equality of the wood surface vapour pressure and the vacuum chamber vapour pressure due to the singularity that arises in the log function. Another boundary constraint for the porous medium system of equations concerns the pressure at the external drying surfaces, which must be fixed at the vacuum chamber pressure. Symmetry planes are introduced into the model to reduce the overall computation times. For the wood sample under consideration here, the computational domain represents only one quarter. Initially the porous medium has some prescribed moisture and temperature distribution, with the pressure being constant throughout at the atmospheric value. The vapour pressure of the chamber and the temperatures of the chamber and the IR emitters are assumed initially to be at ambient conditions.

Numerical Solution Procedure

The numerical procedure used to resolve the coupled model was discussed to some extent in Turner and Perré (2000). Briefly, for the macroscopic transport model, the Finite Volume method is implemented and an efficient Quasi-Newton method (Jennings and McKeown, 1992) used for the temporal resolution of the complicated and often large non-linear system that describes the drying process. The kiln scale system is integrated in time using an implicit first order scheme and the resulting discrete non-linear system analogue $\boldsymbol{\mathcal{F}}(\mathbf{u}) = \left(F_a(\mathbf{u}), F_v(\mathbf{u}), F_w(\mathbf{u}), F_{ch}(\mathbf{u}), F_{IR}(\mathbf{u})\right)^T = \mathbf{0}$ with $\mathbf{u} = \left(\rho_a^{(ch)}, \rho_v^{(ch)}, m_w, T_{ch}, T_{IR}\right)^T$ is solved using Newton's method in order to advance all of the chamber variables in time.

The implicit nature of the integration scheme allows the solution time step to vary throughout the computations, however, care must be taken with this adaptive time stepping strategy to ensure that the gas dynamics evolving in the chamber do not dramatically change throughout any given kiln scale computation. The coupling strategy that exists between the chamber model and the porous medium model is rather complex. This strategy was devised in order to allow the computations of the coupled model to proceed at a time scale that either equals, or is slightly larger than, the time scale required to capture all of the kiln scale phenomena.

RESULTS AND DISCUSSION

In a previous article (Turner and Perré, 2000) the coupled model presented here was validated against an experimental data set for the sapwood part of a Fir tree that was vacuum dried at a surrounding pressure of 20 kPa (boiling point of water ≈ 60°C) using an efficient pump operating at 3 m^3 hr^{-1}. It was remarked that the vacuum drying kinetics closely resembled those observed for high temperature convective drying and it was concluded that the combination of vacuum and IR heating provided an efficient drying process. Furthermore, the trends depicted by the simulations were consistent with those observed experimentally, with the drying time, overpressure and temperature evolution well captured by the double-scale model. This model is now used to study the impact of using a weak pump having one-third the volumetric flow rate of the efficient pump used previously, for the vacuum drying of the same sapwood board. Two case studies are distinguished, the first with a well insulated chamber (see figure 2) and the second with a poorly insulated chamber (see figure 3).

In figure 2(a), for the well insulated chamber, it can be seen that the pump is not always able to keep the pressure in the chamber within the desired range of 0.18 – 0.2 bar, whereas the pump can maintain this range for the poorly insulated chamber exhibited in figure 3(a). It is quite interesting to observe that, when the chamber is poorly insulated, most of the vapour turns into liquid, implying that the vapour flux

eliminated by the pump decreases dramatically. This explains why there is no discernable difference between the results exhibited here for the weak pump and the strong pump case given in Turner and Perré (2000).

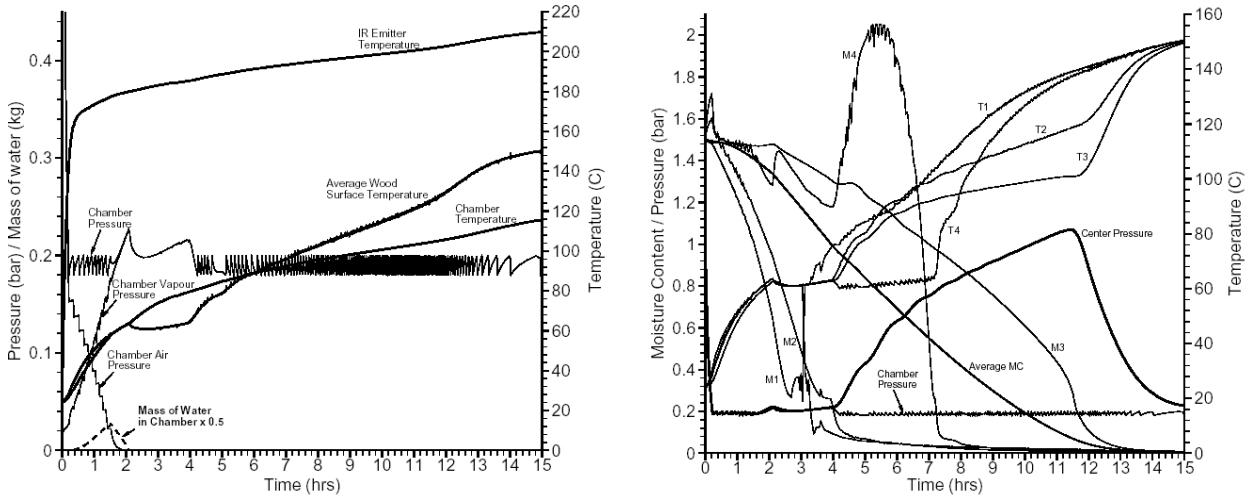

Figure 2 – (a) Evolution of gas dynamics and (b) Drying kinetics in the vacuum chamber for Case Study 1 – Weak pump and well insulated chamber

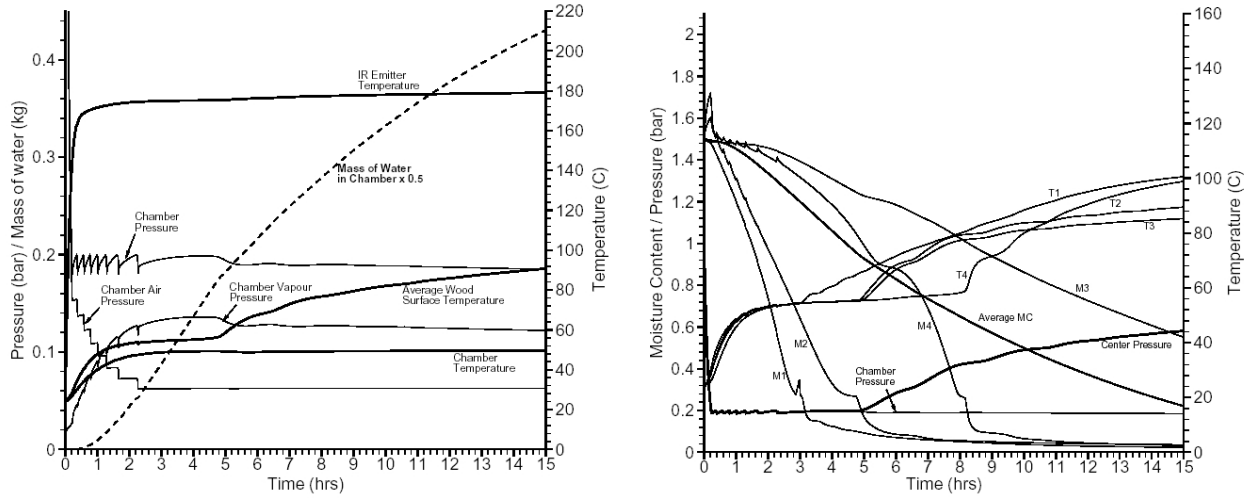

Figure 3 – (a) Evolution of gas dynamics and (b) Drying kinetics in the vacuum chamber for Case Study 2 – Weak pump and poorly insulated chamber

The saturation of the endpiece (M4) and the plateau at the boiling point of the corresponding temperature is remarkable for the well insulated chamber, refer figure 2(b), however, the saturated endpiece can not be observed in figure 3 (b). Indeed, for a poorly insulated chamber, one part of the energy supplied by the IR emitters is just lost through the chamber wall (last term of equation 4). These thermal losses explain why the IR emitter temperature is reduced compared to the well-insulated chamber. As a result, the drying rate is lowered and the internal overpressure reduced and the re-saturation of the endpiece almost disappears.

One may also notice that the intricate coupling induces a certain level of noise for all values calculated at the macro scale, as a result of the vapour pressure variations, hence the change in boiling point, inside the chamber. As usual, the centre pressure starts to increase when the board temperature rises above the

boiling point of water together with a high MC value inside the board. Accordingly, this pressure vanishes when the MC inside the board attains the equilibrium MC. Interestingly, the peak pressure is much lower for the poorly insulated chamber.

One final observation is that the air phase disappears in a step-wise manner at the beginning of the process, decreasing when the pump is switched on and remaining constant when it is off.

Table 1 – Physical constants used for the simulations

Vacuum Chamber Conditions and Material Properties	Values used for the Computations
Initial Moisture Content	150%
Initial Temperature	25 ^{o}C
Porosity	0.733
Density of Solid Matrix	400 kg m^{-3}
Transverse Direction :	
Intrinsic Liquid Permeability	2.10^{-14} m^2
Intrinsic Gas Permeability	4.10^{-15} m^2
Longitudinal Direction :	
Intrinsic Liquid Permeability	5.10^{-12} m^2
Intrinsic Gas Permeability	1.10^{-12} m^2
Wood cross-section	1.3 cm × 22.5 cm× 15 cm
Chamber Characteristics	
Minimum operating pressure	.18 bar
Maximum operating pressure	.20 bar
Volume of chamber	.1 m^3
Dimensions of chamber (cylinder)	radius 0.21 m, height 0.72 m
Mass of IR emitters	2 kg
Mass of Chamber wall	50 kg
Pump flow rate	3 m^3 hr^{-1} efficient pump 1 m^3 hr^{-1} weak pump
External Temperature	25 ^{o}C
External heat transfer coefficient	2.5 W.m^{-2}.°C^{-1} well insulated
Electrical power	300 W

CONCLUSIONS

The two-scale computational model presented here allows the true coupling that exists between the kiln (vacuum chamber) and the load to be accounted for throughout the drying process. Clearly the possibilities of using this tool for designing and optimizing new drying configurations seem endless and the authors hope to explore these possibilities in future research projects. Needless to say, it is only via the use of a sophisticated blend of physical modeling, advanced experimental procedures and state-of-the-art numerical analysis that such a complicated tool can be realized.

LITERATURE

Avramidis, S., (1999), Radio-frequency vacuum drying of wood, Invited Conference, Proceedings of the First COST Action E15 Wood Drying Workshop, 14 pages, Edinburgh, Scotland.

Bird, R.B., Stewart, W.E. and Lightfoot, E.N. 1960), Transport Phenomena, John Wiley and Sons, New York.

Froment, G.F., K.B. Bischoff, (1990), Chemical reactor analysis and design, Series in Chemical Engineering, Wiley, New York.

Jennings, A., and McKeown, J.J. (1992), Matrix Computation, 2nd Edition, Wiley.

Joly P., More Chevalier F., (1980), Théorie, pratique et économie du séchage des bois, H.Vidal éditeur, Paris.

Joyet P., Meunier T., (1996), Drying green Oak under vacuum with superheated steam without discoloration and drawback: industrial results, 5th International IUFRO Wood Drying Conference, 169-176, Québec, Canada.

Masson, E.A., A.P. Malinauskas, (1983), Gas-transport in porous media : the Dusty-Gas model, Chemical Engineering Monographs, 17, Elsevier, Amsterdam.

Perré P. et Degiovanni A. (1990), Simulation par volumes finis des transferts couplés en milieux poreux anisotropes: séchage du bois à basse et à haute température, Int. J. Heat and Mass Transfer, 33(11): 2463-2478.

Perré, P., Moser, M. and Martin M. (1993), Advances in transport phenomena during convective drying with superheated steam or moist air, Int. J. Heat and Mass Transfer, 36(11): 2725-2746.

Perré P., Joyet P. and Aleon D. (1995), Vacuum drying : physical requirements and practical solutions, Tutorial, published in the proceedings of "Vacuum drying of wood '95", 7-34, High Tatras - Slovak Republic.

Perré P., Mosnier S. and Turner I. W. (2004), Vacuum drying of wood with radiative heating: Part I : Experimental procedure with local measurements of temperature and pressure, AIChE, 50(1): 97-107.

Perré P. and Turner I. (1996), Using a set of macroscopic equations to simulate heat and mass transfer in porous media : some possibilities illustrated by a wide range of configurations that emphasize the role of internal pressure " Numerical methods and Mathematical modelling of the Drying Process, 83 - 156, edited by I.W.Turner and A. Mujumdar, Marcel Dekker.

Perré P., and Turner I. W. (1997), Microwave drying of softwood in an oversized waveguide, AIChE Journal, 43(10), 2579-2595.

Perré P. and Turner I. (1999a), TransPore: A Generic Heat and Mass Transfer Computational Model for Understanding and Visualising The Drying Of Porous Media, Invited paper, Drying Technology Journal, 17(7), 1273-1289.

Perré P. and Turner I. (1999b), A 3D version of TransPore : A Comprehensive Heat and Mass Transfer Computational Model for Simulating the Drying of Porous Media" Int. J. Heat Mass Transfer, 42(24), 4501-4521.

Resch H., Gautsch E. (2001), High frequency current/vacuum lumber drying, 7th International IUFRO Wood Drying Conference, 128 – 133, Tsukuba, Japan.

Ressel B. J. (1994), State-of-the-art on vacuum drying of timber, 4th International IUFRO Wood Drying Conference, 255-262, Rotorua, New Zealand.

Rozsa, A. N. and Avramidis S. (1996), Radio frequency vacuum drying of eucalypt timbers, proceedings of the 5th International IUFRO conference, Quebec, Cananda, 135-139.

Tran N. and Rozsa, A.N. (1999), Development of a Novel Radio Frequency Heating System for Drying Wood, proceedings of the 6th International IUFRO conference, Stellenbosch, South Africa, 42-44.

Turner I. and Perré P. (1996), A synopsis of the strategies and efficient resolution techniques used for modelling and numerically simulating the drying process, Numerical methods and Mathematical modelling of the Drying Process, 1 -82, edited by I.W.Turner and A. Mujumdar, Marcel Dekker.

Turner I. and Perré P. (2000), A computational model describing drying kiln dynamics and the coupling with transfer during vacuum drying of wood with radiative heating, Proceedings of the 7th Australasian Heat & Mass Transfer Conference, 3-6/7/00, Townsville, Australia, 335-344.

Whitaker S. (1997), Simultaneous heat, mass, and momentum transfer in porous media: A theory of drying, Advances in Heat Transfer, 13:119-203.